Compressible viscoelasticity: stability of solutions for homogeneous plane-Earth models

Volker Klemann,[1] Patrick Wu[2] and Detlef Wolf[1]

[1]*GeoForschungsZentrum Potsdam, Geodesy and Remote Sensing, Telegrafenberg, D-14473 Potsdam, Germany. E-mail: volkerk@gfz-potsdam.de*
[2]*University of Calgary, Department of Geology & Geophysics, 2500 University Dr NW, Calgary, Alberta, Canada, T2N 1N4. E-mail: ppwu@ucalgary.ca*

SUMMARY
Recently, Purcell has discussed the influence of gravity on load-induced perturbations of compressible, viscoelastic plane-Earth models, where the contributions arising from initial stress and internal buoyancy have been distinguished in the equation of motion. According to his results, the consideration of initial stress is mandatory, whereas that of internal buoyancy has only a minor influence on the solution. We re-examine his study using a different approach. In particular, we present analytical solutions for a homogeneous half-space and discuss the associated relaxation spectra. We show that the solution to the problem involves singularities and branch cuts in the complex *s*-plane in addition to the singularities caused by roots of the determinant function. Furthermore, Rayleigh–Taylor instabilities arising from internal buoyancy cannot be completely balanced by initial stress. Also, the stability margin introduced by Love for an elastic continuum cannot be ignored when applying the solution. Finally, we show that the relaxation spectra can be directly related to the spectral response of a homogeneous, compressible, viscoelastic sphere as studied in recent papers by Vermeersen and Hanyk.

Key words: deformation, dilatation, gravity, normal modes, stability, viscoelasticity.

1 INTRODUCTION

The assumption of small perturbations of the Earth's body is widely used in modelling of geodynamic processes such as seismic waves, post-seismic deformations, glacial-isostatic adjustment or mountain loading. For the latter examples, the quasi-static solutions of the incremental field equations for a radially stratified, gravitating viscoelastic sphere can be represented in the Laplace domain by a discrete spectrum of eigenfunctions or relaxation modes (Peltier 1974, 1976; Wu & Peltier 1982). This representation is analogous to the representation of seismic waves by the discrete spectrum of free oscillations for an elastic sphere, where the acceleration of particles is considered (Alterman *et al.* 1959). A discussion of the analogy between the quasi-static and the dynamic problem has recently been given by Tromp & Mitrovica (1999a). Wolf (1985a) transferred the modal approach to a vertically stratified half-space. The principal characteristics of the relaxation modes of the plane-Earth model were found to be comparable to those of the spherical model.

Recently, the influence of compressibility on the deformations of a viscoelastic Earth has been considered more intensively and the mathematical problems arising for a spherical reference shape have been discussed: in general, compressibility can be separated into material compressibility and internal buoyancy. The former implies that the elastic bulk modulus in the constitutive equation is finite, while the latter refers to the dilatation of the material that causes internal buoyancy (see term III in eq. 1 below). Although this separation cannot be done physically (as both terms will vanish when dilatation is turned off), this is designed for removing instabilities associated with internal buoyancy while keeping compressibility in the material property. If incompressible perturbations are assumed, the solution to the quasi-static viscoelastic problem is represented by a discrete and finite spectrum, where the number of modes depends on the number of layers (Han & Wahr 1995; Vermeersen *et al.* 1996a; Wu & Ni 1996) and on the type of rheology, e.g. whether it is Maxwell or Burgers viscoelasticity (Rümpker & Wolf 1996; Wolf 1997). If compressible perturbations of a spherical model are considered, the number of modes is no longer finite. Han & Wahr (1995) showed the existence of a denumerably infinite set of dilatation modes, the relaxation times of which are inside a finite interval. Vermeersen *et al.* (1996b) gave analytical expressions for these modes, which were later corrected by Hanyk *et al.* (1999).

A corresponding discussion for a plane-Earth model has been lacking so far. Wolf (1985b) noticed that a representation by discrete modes is no longer possible in this case. Therefore, he used a polynomial approximation of the formula for the eigenvalues. Purcell (1998) circumvented the problem arising from a modal approach and used a numerical scheme for the inverse Laplace transformation. In analogy, for

the dynamic problem, continuous spectra appear for acoustic waves in an infinite fluid (e.g. Wilcox 1984) and for surface waves in an elastic half-space (Maupin 1996).

Another problem related to compressibility arises from the assumption of homogeneous density in the reference state. Thus, a compressible viscoelastic perturbation becomes singular in the inviscid limit if initial stress is neglected (Cathles 1975; Wolf 1991b; Wu 1992). Also, if internal buoyancy is considered, Rayleigh–Taylor instabilities appear (Plag & Jüttner 1995). Even at the elastic limit, stability is no longer ensured in the presence of gravity if the elastic restoring forces are below a characteristic stability margin (Jeans 1903; Love 1908; Wieczerkowski 1999). Wolf (1985b) avoided this problem by neglecting the internal-buoyancy term in the field equations for a homogeneous, compressible viscoelastic half-space. Another way to circumvent this problem is to prescribe the density and bulk modulus as functions of depth using the Williamson–Adams equation (Bullen 1975, p. 67), which describes the density increase as a result of the initial stress, and to assume locally incompressible perturbations for the local incremental density (Wolf 1997). From these assumptions, solutions were derived for a viscous sphere by Li & Yuen (1987) and Wu & Yuen (1991), for a viscoelastic half-space by Wolf & Kaufmann (2000) and for a viscoelastic sphere by Martinec *et al.* (2001) and Wolf & Li (2002). For viscoelasticity, it was shown that the relaxation modes correspond to those for incompressible perturbations and that instabilities do not arise.

Similar to the re-examination of perturbations of a homogeneous, compressible viscoelastic sphere by Vermeersen & Mitrovica (2000), here we revisit the problem for a homogenous, compressible half-space recently discussed by Purcell (1998). Because Purcell chose a numerical scheme for the inverse Laplace transformation, he could not study the modal behaviour of the solution. In contrast, using an analytical approach, we are in the position to discuss the stability margin, the relaxation modes and the Rayleigh–Taylor instabilities, which all characterize the physical behaviour of viscoelastic plane-Earth models. Strictly, the Rayleigh–Taylor instability is a fingering instability of an interface between two fluids of different density (Sharp 1984), in the case of the Earth, it is also used, if the density gradient with depth is smaller than the adiabatic one (Plag & Jüttner 1995). The physical cause of elastic instability and the stability margin was further discussed by Rayleigh (1906) and Love (1911). In order to obtain the solution in the time domain, the contour of integration in the inverse Laplace transformation must be distorted to include the contributions of branch cuts. One of the objectives of this paper is to document the existence of such non-analyticities and to evaluate their effects on the incremental gravity and the vertical and horizontal displacements in the wavenumber and time domains. Another objective is to understand the energy balance associated with viscoelastic instabilities.

2 FIELD EQUATIONS

The incremental momentum equation for quasi-static perturbations of a homogeneous, viscoelastic gravitating continuum is

$$\underbrace{\boldsymbol{\nabla} \cdot \mathbf{t}^{(\delta)}}_{\text{I}} + \underbrace{\boldsymbol{\nabla}(\mathbf{u} \cdot \boldsymbol{\nabla} p^{(0)})}_{\text{II}} - \underbrace{\rho^{(0)}\mathbf{g}^{(0)}\boldsymbol{\nabla} \cdot \mathbf{u}}_{\text{III}} + \underbrace{\rho^{(0)}\mathbf{g}^{(\Delta)}}_{\text{IV}} = \mathbf{0}, \tag{1}$$

where $\mathbf{t}^{(\delta)}$ is the material incremental Cauchy stress, $\mathbf{u}$ is the displacement, $p^{(0)}$ is the reference pressure, $\rho^{(0)}$ is the reference volume-mass density, $\mathbf{g}^{(0)} = g^{(0)} \mathbf{e}_z$ is the reference gravity, with being $\mathbf{e}_z$ directed vertically downwards and $\mathbf{g}^{(\Delta)}$ is the local incremental gravity. We use the Lagrangian representation, which distinguishes between the reference value of a field quantity, $f^{(0)}(\mathbf{X})$, its local increment, $f^{(\Delta)}(\mathbf{X}, t)$, describing the change at the reference position $\mathbf{X}$, and its material increment, $f^{(\delta)}(\mathbf{X}, t)$, describing the change of the material point at the current position $\mathbf{r}(\mathbf{X}, t) = \mathbf{X} + \mathbf{u}\,(\mathbf{X}, t)$ (Wolf 1991a). The material incremental Cauchy stress can be expressed by

$$\mathbf{t}^{(\delta)}(t) = \left[\kappa - \frac{2}{3}m(0)\right]\mathbf{1}\boldsymbol{\nabla} \cdot \mathbf{u}(t) + 2m(0)\boldsymbol{\epsilon}(t) + 2\int_0^t \left[\boldsymbol{\epsilon}(t - t') - \frac{1}{3}\mathbf{1}\boldsymbol{\nabla} \cdot \mathbf{u}(t - t')\right]d_{t'}m(t')\,dt', \tag{2}$$

which is the incremental constitutive equation for linear viscoelasticity, where t is the current time, t' is the excitation time, $\boldsymbol{\epsilon}$ is the infinitesimal strain, $\boldsymbol{\epsilon} := \frac{1}{2}(\boldsymbol{\nabla}\mathbf{u} + \boldsymbol{\nabla}\mathbf{u}^\mathrm{T})$, κ is the elastic bulk modulus and $m(t)$ is the shear-relaxation function. For a Maxwell fluid, it is given by

$$m(t) = \mu^\mathrm{E}\mathrm{e}^{-t/\tau} \quad \text{with} \quad \tau := \frac{\eta}{\mu^\mathrm{E}}, \tag{3}$$

where μ^E is the shear modulus, τ is the Maxwell time and η is the dynamic viscosity. The local incremental gravity is related to the local incremental potential, $\phi^{(\Delta)}$, by

$$\mathbf{g}^{(\Delta)} := \boldsymbol{\nabla}\phi^{(\Delta)}. \tag{4}$$

The incremental potential equation is

$$\nabla^2\phi^{(\Delta)} = 4\pi\gamma\rho^{(0)}\boldsymbol{\nabla} \cdot \mathbf{u} \tag{5}$$

where γ is the gravitational constant.

In eq. (1), we distinguish the following terms.

(I) The *viscoelastic force* can be decomposed according to three time intervals: (a) the instantaneous elastic response governed by the elastic bulk modulus, κ, and the shear modulus, μ^E, (b) the relaxation of shear forces on the timescale of the Maxwell time, τ, and (c) the linear creep of a Newtonian-viscous fluid controlled by the dynamic viscosity, η.

(II) The *advective force* is related to the displacement of particles with respect to the initial stress field.

(III) The *buoyancy force* is related to local density perturbations caused by dilatation.

(IV) The *gravitational force* is related to local gravity perturbations and couples the momentum eq. (1) with the potential eq. (5).

In the following, we neglect term IV and, thus, the coupling of eq. (1) and eq. (5). To distinguish the influence of the individual terms I–III on the behaviour of the solution, we consider four simplifications.

I $= 0$ (approximation C0): this represents the classical Boussinesq problem without gravitational forces (e.g. Jeffreys 1959, p. 27; Farrell 1972; Cathles 1975, p. 57). Since there are no restoring forces at the inviscid limit, the approximation is of interest only to the elastic case.

I $+$ II $= 0$ (approximation C1): this allows the initial stress to be a restoring force, which also applies at the inviscid limit.

I $+$ II $+$ III $= 0$ (approximation C2): this also includes internal buoyancy, which counteracts the initial stress.

I $+$ II $= 0$ and $\lim \kappa \to \infty$ (approximation IC): this represents the incompressible limit of approximations C1 and C2.

Applying the Laplace transformation:

$$\tilde{f}(s) := \int_0^\infty f(t) e^{-st}\, dt, \tag{6}$$

the momentum eq. (1) is

$$\underbrace{\nabla \cdot \tilde{\mathbf{t}}^{(\delta)}}_{\mathrm{I}} + \underbrace{\nabla\left[\tilde{\mathbf{u}} \cdot \nabla p^{(0)}\right]}_{\mathrm{II}} - \underbrace{\rho^{(0)}\mathbf{g}^{(0)}\nabla \cdot \tilde{\mathbf{u}}}_{\mathrm{III}} = \mathbf{0}, \tag{7}$$

where we already have neglected term IV, and the constitutive eq. (2) formally reduces to Hooke's law:

$$\tilde{\mathbf{t}}(s) = \left[\kappa - \frac{2}{3}\tilde{\mu}(s)\right]\nabla \cdot \tilde{\mathbf{u}}(s)\mathbf{1} + 2\tilde{\mu}\tilde{\boldsymbol{\epsilon}}(s) \tag{8}$$

with the relaxation modulus for Maxwell viscoelasticity:

$$\tilde{\mu}(s) := s\tilde{m}(s) = \frac{\mu^{\mathrm{E}}}{1 + (s\tau)^{-1}}. \tag{9}$$

Assuming the material parameters to be homogeneously distributed, a combination of eqs (7) and (8) yields

$$\underbrace{\tilde{\mu}\nabla^2\tilde{\mathbf{u}} + \left(\kappa + \tfrac{1}{3}\tilde{\mu}\right)\nabla\nabla \cdot \tilde{\mathbf{u}}}_{\mathrm{I}} + \underbrace{\rho^{(0)}g^{(0)}\nabla(\tilde{\mathbf{u}} \cdot \mathbf{e}_z)}_{\mathrm{II}} - \underbrace{\rho^{(0)}g^{(0)}\mathbf{e}_z\nabla \cdot \tilde{\mathbf{u}}}_{\mathrm{III}} = \mathbf{0}. \tag{10}$$

For axial symmetry and cylindrical coordinates, we can recast the problem into a homogeneous, linear system of four first-order differential equations:

$$\frac{d}{dz}\tilde{\mathbf{Y}}(k, z, s) = \mathbf{A}(k, s)\tilde{\mathbf{Y}}(k, z, s) \tag{11}$$

with the solution vector, $\tilde{\mathbf{Y}} = [-\tilde{U}, \tilde{W}, -\tilde{R}, \tilde{T}]^{\mathrm{T}}$, in terms of the Hankel-transformed horizontal and vertical displacements and the Hankel-transformed horizontal and vertical components of normal traction $\tilde{\mathbf{t}}\cdot\mathbf{e}_z$, respectively, the Hankel wavenumber k and the downward coordinate z (Singh 1970). In the following, when referring to field quantities, Hankel transformation is always implied. The coefficient matrix, $\mathbf{A}$, depends on the approximation of the momentum equation considered:

$$\mathbf{A} := \begin{pmatrix} 0 & -k & \dfrac{1}{\tilde{\mu}} & 0 \\[2mm] \dfrac{\tilde{\lambda}k}{\tilde{\lambda} + 2\tilde{\mu}} & 0 & 0 & \dfrac{1}{\tilde{\lambda} + 2\tilde{\mu}} \\[2mm] \dfrac{4\tilde{\mu}(\tilde{\lambda} + \tilde{\mu})k^2}{\tilde{\lambda} + 2\tilde{\mu}} & -\delta_{\mathrm{II}}\rho^{(0)}g^{(0)}k & 0 & -\dfrac{\tilde{\lambda}k}{\tilde{\lambda} + 2\tilde{\mu}} \\[2mm] -\dfrac{(\delta_{\mathrm{II}}\tilde{\lambda} + \delta_{\mathrm{III}}2\tilde{\mu})\rho^{(0)}g^{(0)}k}{\tilde{\lambda} + 2\tilde{\mu}} & 0 & k & -\dfrac{(\delta_{\mathrm{II}} - \delta_{\mathrm{III}})\rho^{(0)}g^{(0)}}{\tilde{\lambda} + 2\tilde{\mu}} \end{pmatrix}, \tag{12}$$

where $\tilde{\lambda} := \kappa - 2/3\tilde{\mu}$ and δ_{II} and δ_{III} are the switches for initial stress and internal buoyancy, respectively. Their values are one if the corresponding term is considered and zero otherwise (e.g. Purcell 1998). For approximation IC, $\tilde{\lambda} \to \infty$ must be applied.

From matrix $\mathbf{A}$, the eigenvalues and eigenvectors for the four approximations are obtained using the conventional approach. The results are summarized in Appendix A. Inspection of eq. (A22) shows that, even for the elastic case, the eigenvalues m_2 and m_4 of approximation C2 become complex if k is small. As discussed in Section 3, this results in a stability margin, which was noted by Love (1908). For the viscoelastic case (when $\tilde{\lambda}$ and $\tilde{\mu}$ are functions of the Laplace-transform variable s), eqs (A12) and (A22) show that the eigenvalues of approximations C1 and C2 involve square roots. Thus, branch cuts and branch points exist and the path of integration on the complex plane must be distorted when implementing the inverse Laplace transformation to obtain the solution in the time domain. That is discussed in more detail in Section 4. From the eigenvectors, the fundamental matrix and the solution vector can be constructed. The latter is given by

$$\tilde{\mathbf{Y}}(z) = A_3\mathbf{L}_3 e^{m_3 z} + A_4\mathbf{L}_4 e^{m_4 z}, \tag{13}$$

where $\mathbf{L}_{3,4}$ are the third and fourth columns of the fundamental matrix, $\mathbf{L}$, calculated from the fundamental system, $\mathbf{AL} - \mathbf{Lm} = \mathbf{0}$, given in Appendix A for the different approximations and $\mathbf{m}$ is the Jordan normal form containing the eigenvalues m_i. The third and fourth column

with $m_{3,4} \in \{m_i | \operatorname{Re} m_i < 0\}$ are chosen to fulfil the regularity condition for $z \to \infty$ that all increments must vanish. The real parts of $m_{1,2}$ are positive and, thus, violate the regularity condition. The factors $A_{3,4}$ are calculated from the boundary conditions. If we assume a surface load as excitation, $[\tilde{R}, \tilde{T}](z = 0) = [0, -g^{(0)}\tilde{\Sigma}]$, we obtain

$$A_{3,4} = -\frac{g^{(0)}\tilde{\Sigma}}{\det \mathbf{M}}[-L_{34}, L_{33}], \tag{14}$$

where $\tilde{\Sigma}$ is the Hankel-transformed surface-mass density and

$$\mathbf{M} = \begin{pmatrix} L_{33} & L_{34} \\ L_{43} & L_{44} \end{pmatrix}. \tag{15}$$

Of interest is also the local incremental gravity, which corresponds approximately to the free-air gravity anomaly. Since it does not enter into the momentum equation, it can be calculated directly from the potential equation. We write eqs (4) and (5) as an inhomogeneous first-order system of differential equations:

$$\partial_z \mathbf{Z}(z) = \mathbf{B}\mathbf{Z}(z) + \mathbf{F}(z) \tag{16}$$

with

$$\mathbf{B} = \begin{pmatrix} 0 & 1 \\ k^2 & 0 \end{pmatrix}, \qquad \mathbf{Z} = \begin{pmatrix} \tilde{\Phi} \\ \tilde{G} \end{pmatrix}, \qquad \mathbf{F} = \begin{pmatrix} 0 \\ 4\pi\gamma\rho^{(0)}\tilde{D} \end{pmatrix}, \tag{17}$$

where $\tilde{\Phi}$ and $\tilde{G}$ represent the Hankel-transformed local incremental potential and gravity, respectively, and $\tilde{D} = \partial_z \tilde{W} - k\tilde{U}$ is the Hankel-transformed dilatation. The formal solution to eq. (17):

$$\mathbf{Z}(z) = \mathrm{e}^{\mathbf{B}(z-z_0)}\mathbf{Z}(z_0) + \int_{z_0}^z \mathrm{e}^{\mathbf{B}(z-z')}\mathbf{F}(z')\,dz' \tag{18}$$

is calculated using the propagator-matrix method (e.g. Gantmacher 1986, p. 143). After consideration of regularity and some manipulations, we arrive at

$$\begin{pmatrix} \tilde{\Phi}(z_1) \\ \tilde{G}(z_1) \end{pmatrix} = \begin{pmatrix} 1/k \\ 1 \end{pmatrix} 2\pi\gamma \left[\tilde{\Sigma} - \rho^{(0)}\tilde{W}(z_1) + \rho^{(0)}\overline{D} \right], \tag{19}$$

where

$$\bar{D} := \frac{A_3}{m_3 - k}\frac{L_{43} - 2\tilde{\mu}kL_{13}}{\tilde{\lambda} + 2\tilde{\mu}} + \frac{A_4}{m_4 - k}\frac{L_{44} - 2\tilde{\mu}kL_{14}}{\tilde{\lambda} + 2\tilde{\mu}} \tag{20}$$

considers the contribution caused by dilatation. From eqs (13), (14), (19) and (20) and the explicit form of the fundamental matrices and eigenvalues, we can then derive closed-form representations of the solution vector for the different approximations (Appendix A).

3 ELASTIC HALF-SPACE

In this section, we study the effects of internal buoyancy and initial stress on the displacement, incremental gravity and energy for an elastic half-space. Of particular interest is the physical interpretation of instabilities, as revealed in the eigenvalues for approximation C2. We use energy potentials to study unstable equilibrium states. The formulae for the displacement and incremental gravity of the four approximations are given in Appendix A, the energy contributions are derived in Appendix C. For convenience, we introduce the normalized wavenumber, $n := ka$, where a is the Earth's radius, so that n corresponds to the Legendre degree for spherical geometry. Setting $\Sigma = \rho^{(0)}$ in the expressions of Appendix A, we also normalize the displacements with respect to the vertical surface displacement for an incompressible fluid at the inviscid limit. For the elastic case, the constitutive equation is given by Hooke's law. We may thus neglect the tildes in the equations and replace the relaxation modulus by the shear modulus. Table 1 presents the parameters chosen for the following calculations. Examining the displacements of the four approximations (Fig. 1) the most important feature is the vanishing of the horizontal displacement, U, at the surface for the incompressible approximation IC (Fig. 1a). This results from eqs (A7), (A17) and (A26), which show that $U \propto 1 - 2\nu$ (e.g. Farrell 1972), where the Poisson ratio $\nu = \frac{1}{2}$ and $\lambda \to \infty$ for approximation IC. The positive values of U for the other approximations result from the definition of the solution vector, $\mathbf{Y} = [-U, W, -R, T]$. Thus, positive values result in a displacement towards the origin.

For the vertical displacement, W (Fig. 1b), we have $W \propto 2(1 - \nu)$ according to eqs (A8), (A18) and (A27). This results in systematically smaller displacements for approximation IC than for the compressible approximations where $\nu < \frac{1}{2}$. For small wavenumbers, the compressible approximations C1 and C2 differ from approximation C0 because of the differences in how gravity is considered (Figs 1b and c). Furthermore, comparing eqs (A8) and (A18), we see that, for the vertical displacement, the initial stress due to $\rho^{(0)}g^{(0)}$ reduces the displacement, while the additional terms in eq. (A27) due to internal buoyancy increase it.

Table 1. Parameter values for homogeneous plane-Earth model.

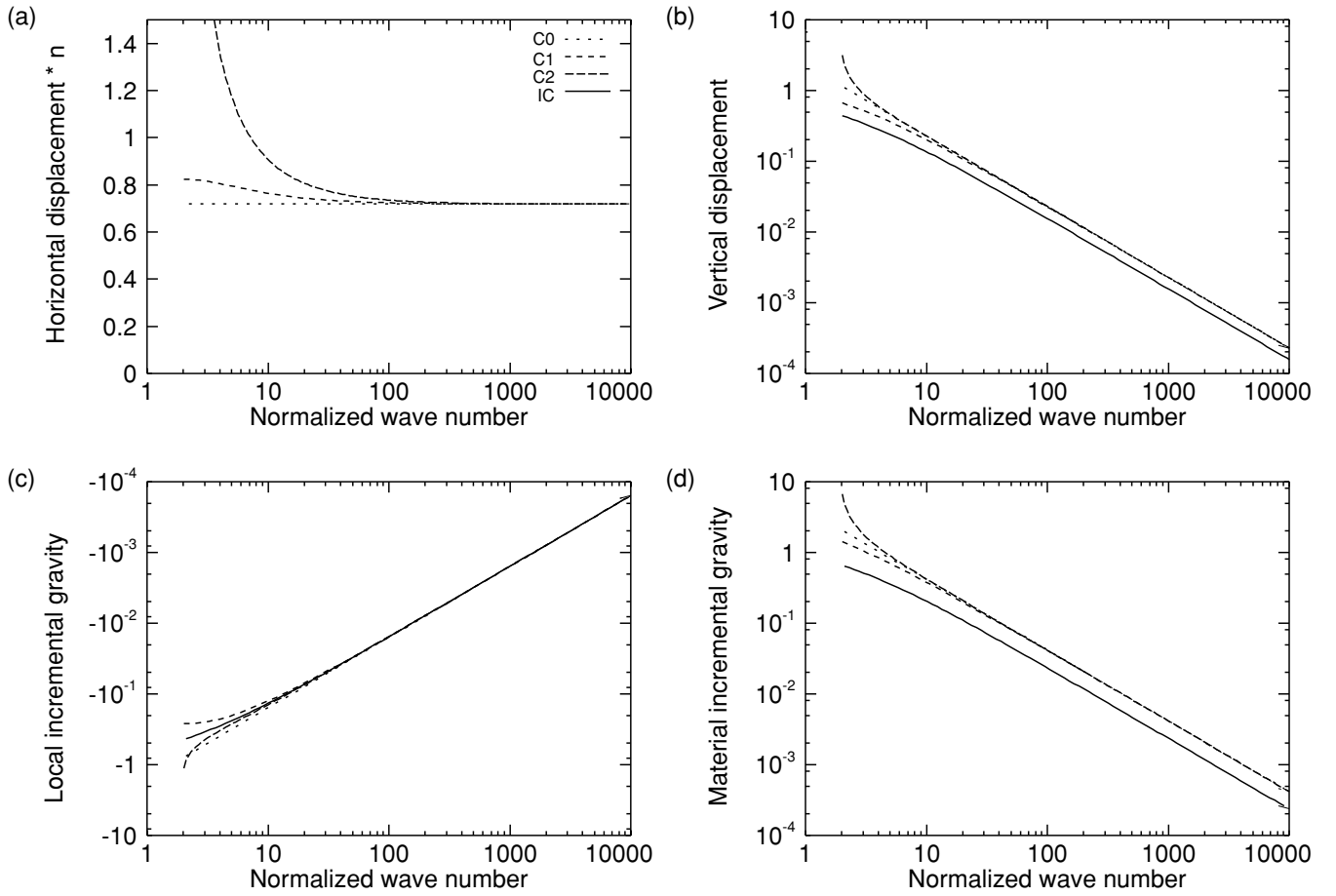| $\rho^{(0)}$ (kg m^{-3})	κ (GPa)	μ^{E} (GPa)	η (Pa s)
3380	124.7	67.0	10^{21}

Figure 1. Displacement and incremental gravity at the elastic limit for approximations C0, C1, C2 and IC as functions of normalized wavenumber, n. (a) shows the horizontal surface displacement, nU, which is zero for approximation IC, (b) shows the vertical (downward) surface displacement, W, (c) the local incremental gravity, $G^{(\Delta)}$, and (d) the material incremental gravity, $G^{(\delta)}$. In (c) and (d) the contribution of the load is subtracted. The displacement is normalized with respect to the downward displacement in the hydrostatic equilibrium, $\Sigma/\rho^{(0)}$, the gravity with respect to the gravity associated with the surface load, $2\pi\gamma\Sigma$.

A complication appears for approximation C2 and $n > 3$, where the vertical displacement becomes greater than 1. This means that the displacement is greater than the value at the inviscid limit, where equilibrium applies. For n smaller than a critical wavenumber, n_{crit}, the eigenvalues $m_{2,4}$ given in (A22) are imaginary. Thus, according to eq. (13), the displacements oscillate harmonically with depth and thus violate the regularity condition. Love (1911) called this change of behaviour the stability margin. Setting $\epsilon = 1$ in eq. (A21), the stability margin is

$$n_{crit} = \frac{\rho^{(0)}g^{(0)}a}{\sqrt{\mu^{E}(\kappa + \frac{4}{3}\mu^{E})}}. \tag{21}$$

For the parameters in Table 1, $n_{crit} = 1.7$ and, therefore, an unstable solution exist for smaller values. However, such small values are far beyond the validity of the half-space approximation for the Earth. Figs 1(a) and (b) also demonstrate that the effects of internal buoyancy and initial stress decrease with increasing wavenumber. Consequently, only material compressibility remains significant at short wavelengths.

For the local incremental gravity, $G^{(\Delta)}$, we observe in Fig. 1(c) that, besides the influence of gravity for small wavenumbers, the behaviour is very similar for all four approximations. This means that decreasing gravity due to downward displacement is compensated by increasing gravity due to compression. In Fig. 1(d), the material incremental gravity, $G^{(\delta)}$, is plotted, which represents the perturbation at the displaced surface. This quantity can be derived from the solution, considering in a first approximation an advective increment that describes the change of gravity caused by the shift in the reference field: $G^{(\delta)} = G^{(\Delta)} + \partial_z g^{(0)} W$. Of course the gradient has to be prescribed, because the gravitational potential cannot be calculated self-consistently for a half-space. Since the advective contributions dominate, the incompressible limit now differs from the compressible approximations.

Another interesting feature appears if we analyse the energy terms contributing to the deformation (Tromp & Mitrovica 1999b; Klemann & Wolf 1999). For this, we consider the energy equation

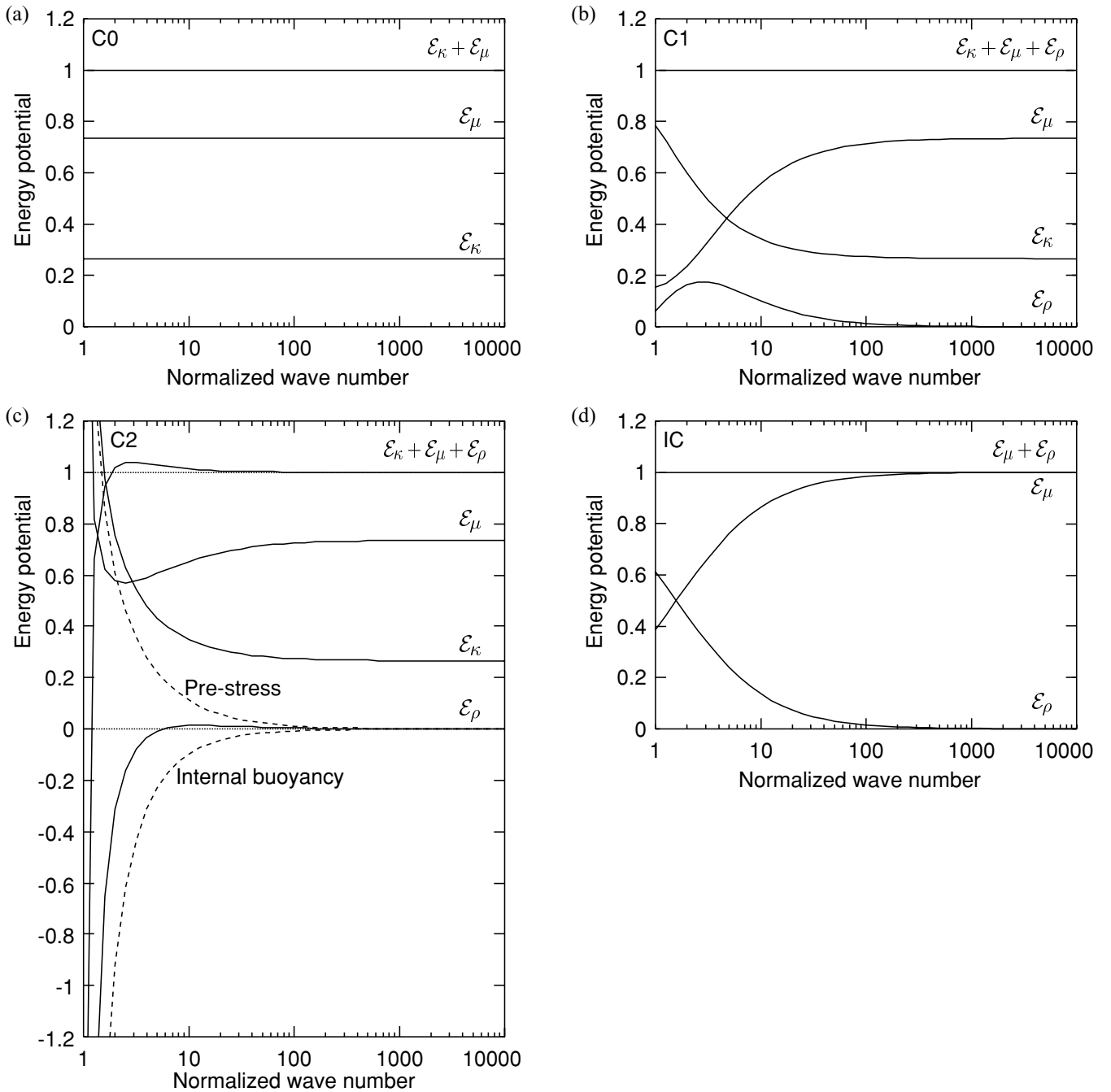$$\mathcal{E}_\sigma + \mathcal{E}_\kappa + \mathcal{E}_\mu + \mathcal{E}_\rho = 0 \tag{22}$$

Figure 2. Energy potentials $\mathcal{E}_\kappa$, $\mathcal{E}_\mu$ and $\mathcal{E}_\rho$ at the elastic limit for approximations C0, C1, C2 and IC as functions of normalized wavenumber, n, and normalized to the excitation potential, $\mathcal{E}_\sigma$.

where $\mathcal{E}_\sigma$ is the excitation energy associated with the loading of the surface, $\mathcal{E}_\kappa$ is the bulk energy, $\mathcal{E}_\mu$ is the shear energy and $\mathcal{E}_\rho$ is the gravitational energy (see Appendix C for their explicit expressions). Fig. 2 shows the energy contributions for the different approximations calculated from eqs (C5)–(C11), with the displacements as functions of depth inserted. For approximation C0 (Fig. 2a) and approximation IC (Fig. 2d), the behaviour is obvious: in the first case, we obtain $\mathcal{E}_\kappa/\mathcal{E}_\mu = (1 - \nu - 2\nu^2)/(1 - \nu + \nu^2)$ and $\mathcal{E}_\rho$ is irrelevant. Also, from $0 < \nu \leq \frac{1}{2}$ (e.g. Landau & Lifschitz 1989, p. 16), it follows that $\mathcal{E}_\mu \geq 2\mathcal{E}_\kappa$. In the second case we obtain $\mathcal{E}_\rho/\mathcal{E}_\mu = \rho^{(0)}g^{(0)}a/(2n\mu^E)$, which confirms the vanishing influence of gravity for increasing n. For approximations C1 and C2, the behaviour is more complicated and an analytical representation of the energy ratios is not illuminating. For $n \to \infty$, the influence of gravity vanishes and approximations C1 and C2 behave as C0. For smaller n and approximation C1 (Fig. 2b), we find a similar increase of $\mathcal{E}_\rho$ as for approximation IC. However, for a further decrease in n, $\mathcal{E}_\rho$ reaches a maximum and then decreases, whereas the contribution of $\mathcal{E}_\kappa$ becomes dominant. This means that the influence of the divergence of the displacement in $\mathcal{E}_\kappa$ dominates that of the displacement gradient in $\mathcal{E}_\rho$.

For approximation C2 (Fig. 2c), two almost compensating contributions to $\mathcal{E}_\rho$, those due to initial stress and internal buoyancy, must be considered. Since the internal-buoyancy energy is negative, $\mathcal{E}_\rho$ is almost negligible, becomes negative for $n < 5$ and diverges for $n \to n_{\mathrm{crit}}$ when the internal buoyancy becomes dominant. At this limit, the contributions $\mathcal{E}_\kappa$ and $\mathcal{E}_\mu$ diverge to $+\infty$, which corresponds to the divergent displacements in Figs 1(a) and (b). A second feature of this model is that the internal energy, $\mathcal{E}_\kappa + \mathcal{E}_\mu + \mathcal{E}_\rho$, is not equal to $-\mathcal{E}_\sigma$. For $n > 2$, it is slightly greater than the excitation energy and, for $n < 2$ and $n \to n_{\mathrm{crit}}$, it tends to $-\infty$. This behaviour results from the fact that the displacements governed by eq. (10) correspond to disturbances of an unstable reference state.

4 VISCOELASTIC HALF-SPACE

The viscoelastic field equations, which describe the rheological behaviour of the half-space, are solved in the Laplace domain. In order to predict the temporal behaviour of the different approximations, we implement the inverse Laplace transformation using the residue theorem (Wu 1978; Peltier 1985). This allows us to replace the Bromwich path of integration by the sum of the residues calculated from the non-analytic regions of the solution in the complex s-plane. If there are only simple and isolated poles, s_i, the solution is represented by the relaxation modes, and the solution for a Heaviside excitation, $h(t)$, is

$$\mathbf{Y}(t) * h(t) = \mathbf{Y}^{\mathrm{E}} + \sum_i \mathrm{Res}\left[\tilde{\mathbf{Y}}(s)\frac{1}{s}\left(e^{st} - 1\right)\right]_i = \mathbf{Y}^{\mathrm{E}} + \sum_i \mathbf{Y}_i^{\mathrm{V}}\left(1 - e^{s_i t}\right) \tag{23}$$

where $\mathbf{Y}^{\mathrm{E}}$ is the elastic amplitude, $\mathbf{Y}_i^{\mathrm{V}} := -\mathrm{Res}[\tilde{\mathbf{Y}}(s)/s]_i$ is the ith viscous amplitude and $-1/s_i$ is the corresponding relaxation time. We calculate the amplitudes using the Heaviside theorem:

$$\mathrm{Res}\left[\tilde{\mathbf{Y}}(s_i)\right] = \mathrm{Res}\left[\frac{\mathbf{g}(s_i)}{h(s_i)}\right] = \left.\frac{\mathbf{g}(s)}{\partial_s h(s)}\right|_{s=s_i}, \tag{24}$$

where the components of $\tilde{\mathbf{Y}}$ can be represented by the fraction of two analytic functions, $\mathbf{g}(s)$ and $h(s)$, with $h(s)$ having simple roots at s_i (e.g. Arfken 1985, p. 400). Considering (14), s_i are the roots of det $\mathbf{M}$ and the expression 'normal modes' is motivated (Peltier 1976). However, this is only valid for approximation IC. Since the spectral behaviour of this approximation has already been discussed (e.g. Wolf 1997), we only summarize its main features. For approximation IC, we have one relaxation mode M with the relaxation time $\tau[1 + 2n\mu^{\mathrm{E}}/(\rho^{(0)}g^{(0)}a)]$. The horizontal surface displacement is zero. For the vertical displacement, the amplitude at the inviscid limit is one and the amplitude of mode M is just the difference between the inviscid amplitude and the elastic amplitude, see eq. (23). According to eq. (19) and because $\bar{D} = 0$, the local incremental gravity is proportional to the vertical displacement.

As mentioned in Section 2, approximation C0 cannot be used in the case of Maxwell viscoelasticity, because no restoring forces are present at the inviscid limit. For approximations C1 and C2, we identify square-root terms in the expressions (A12) and (A22) for the eigenvalues, which imply branch points and cut lines as continuous non-analytic regions in the complex s-plane, as discussed in Appendix B. Of course the square-root terms also appear in the corresponding det $\mathbf{M}$, eqs (A13) and (A23). These regions coincide with s values, for which the square roots in the expressions (A12) and (A22) for the eigenvalues are imaginary. For approximation C1, the non-analytic behaviour is shown in Fig. 3(a), where we distinguish the branch points $s_{1,2}^{\mathcal{B}}$, which are complex conjugate, $s_3^{\mathcal{B}}$ and the connecting branch cuts $\mathcal{C}_{1,2}$. For $n \to \infty$, $s_{1,2}^{\mathcal{B}}$ converge to $s_3^{\mathcal{B}}$, see eq. (B1) and Fig. 3(b).

In addition to the non-analyticities arising from the eigenvalues and eigenvectors, there are simple poles in $1/$ det $\mathbf{M}$, which give rise to the modes M and CP. Note that mode CP was called mode T by Wolf (1985b), describing the transition from the elastic response to the viscous response (Cathles 1975, p. 57). The latter is described by mode M. The relaxation times of these modes are plotted in Fig. 4(a) and the displacement and incremental gravity are shown in Figs 4(b)–(d). The dashed lines reflect contributions from the real part of the numerical integration along the contour around the branch points $s_{1,2}^{\mathcal{B}}$ and $s_3^{\mathcal{B}}$ shown in Fig. 3(a). We call this region continuous mode D, in accordance with the results for a homogeneous, compressible sphere by Vermeersen *et al.* (1996b) (Section 5). As for approximation IC, the amplitude of mode M dominates the vertical displacement (Fig. 4c) and, together with those of modes CP, D and the elastic amplitude, E, sum up to the inviscid amplitude, $\Sigma = F$. However, unlike the incompressible case, the horizontal amplitudes of the modes are no longer zero (Fig. 4b). Since $D \neq 0$ in (19), the local incremental gravity does not vanish at the inviscid limit (Fig. 4d).
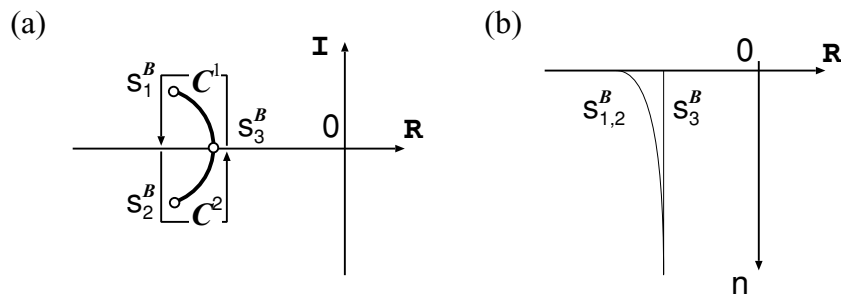

Figure 3. (a) Branch cuts and branch points of $\sqrt{1 + \epsilon(s)^2}$ for approximation C1 in the complex s-plane and (b) real parts of branch points as functions of normalized wavenumber, n.
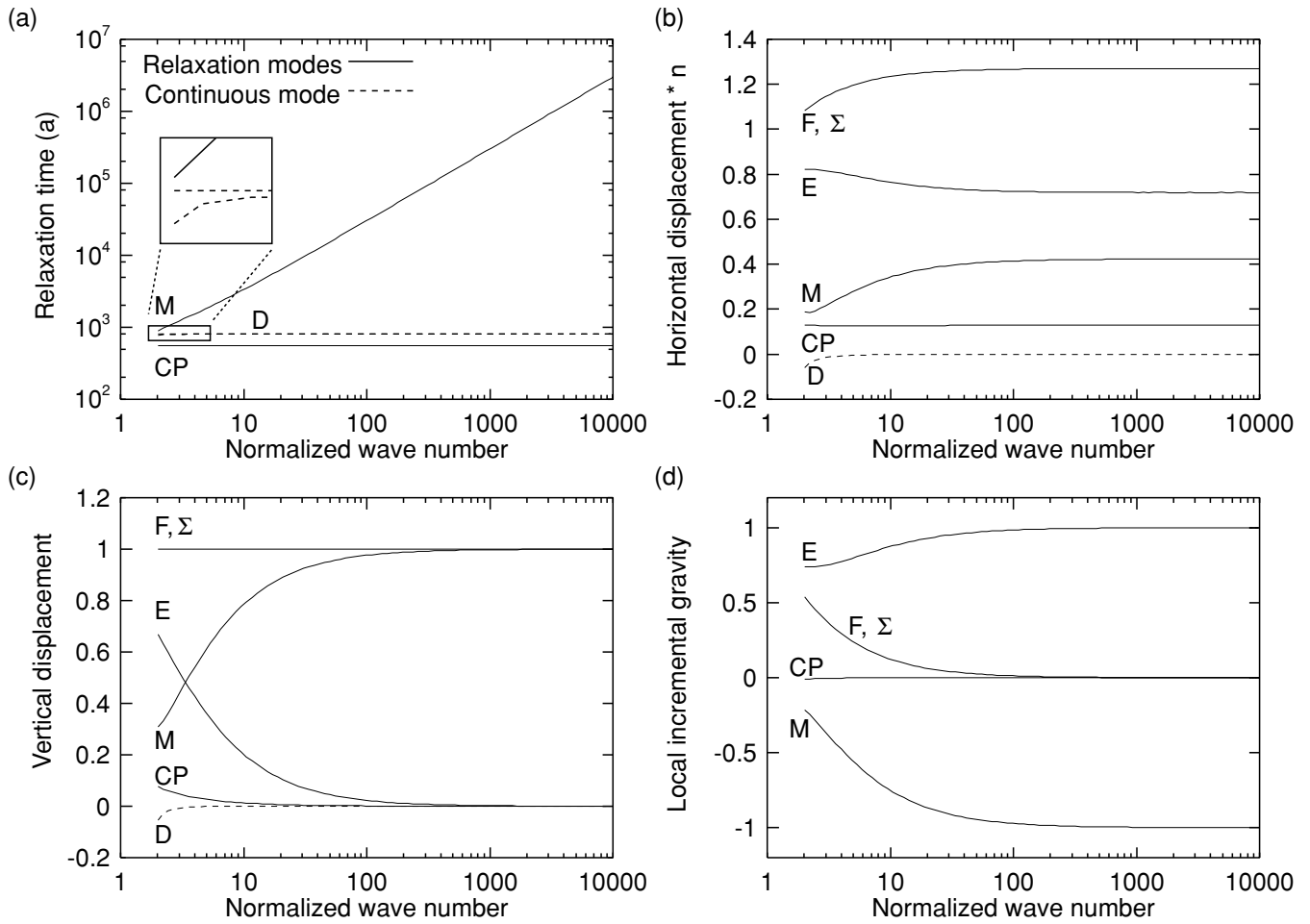
Figure 4. (a) Relaxation-time spectrum and (b)–(d) horizontal and vertical surface displacements and local incremental gravity, respectively, for approximation C1 as functions of normalized wavenumber, n. Horizontal displacements are multiplied by n. The relaxation modes M and CP and their amplitudes, the elastic amplitude, E, their sum, Σ, and the inviscid amplitude, F, are shown by solid lines, the branch points of the continuous mode D and its amplitude by dashed lines. The normalizations are as for Fig. 1. The insert in (a) discriminates the two branch points of mode D. In contrast to Fig. 1(c), the contribution due to the load is included in (d).
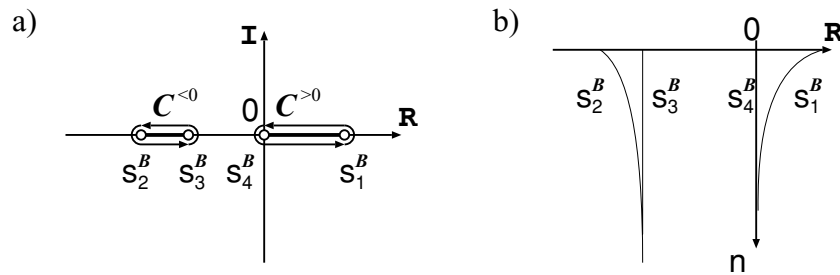

Figure 5. (a) Branch cuts and branch points of $\sqrt{1 - \epsilon(s)}$ for approximation C2 in the complex s-plane and (b) real parts of branch points as functions of normalized wavenumber, n.

Next, we consider approximation C2. Fig. 5(a) shows two branch cuts, $\mathcal{C}^{>0}$ and $\mathcal{C}^{<0}$, appearing for this approximation and the corresponding pairs of branch points, $s_{1,4}^{\mathcal{B}}$ and $s_{2,3}^{\mathcal{B}}$. Fig. 5(b) shows that, for $n \to \infty$, pairs of branch points converge: $s_1 \to s_4$ and $s_2 \to s_3$. The relaxation-time spectrum (Fig. 6a) shows the relaxation modes M and CP. The branch cut $\mathcal{C}^{<0} \subset \mathcal{R}$ is restricted to a narrow region in the vicinity of mode CP. Because, according to eqs (B3) and (B7), $s_3^{\mathcal{B}}$ is identical for approximations C1 and C2, we also call this branch cut continuous mode D. In contrast, $s_{1,2}^{\mathcal{B}}$ for approximation C1 and $s_2^{\mathcal{B}}$ for approximation C2 differ, see eqs (B1) and (B5).

The branch cut $\mathcal{C}^{>0} \subset \mathcal{R}$ extends from $s_4^{\mathcal{B}} = 0$ to $s_1^{\mathcal{B}} > 0$, see eqs (B5)–(B8). Fig. 6(a) shows its upper bound as $1/s_1^{\mathcal{B}}$. Its lower bound would be at infinite times in this representation, so that $\mathcal{C}^{>0}$ fills the region above $1/s_1^{\mathcal{B}}$. Because of the destabilizing character of $\mathcal{C}^{>0}$, we call this branch cut the continuous mode RT. It corresponds with the Rayleigh–Taylor modes found by Plag & Jüttner (1995) for a compressible
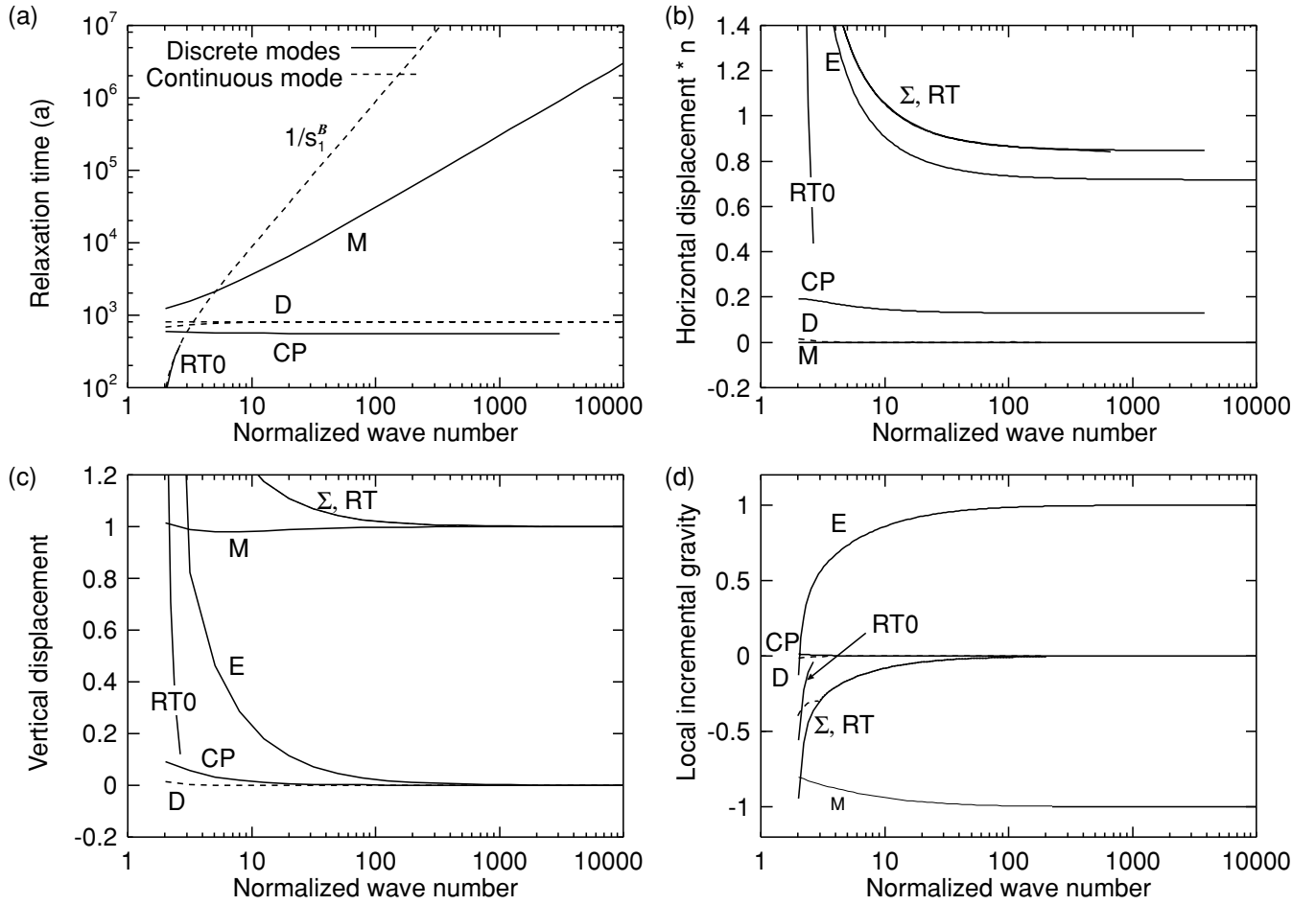
Figure 6. (a) Relaxation-time spectrum and (b)–(d) horizontal and vertical surface displacements and local incremental gravity, respectively, for approximation C2 as functions of normalized wavenumber, n. Horizontal amplitudes are multiplied by n. The relaxation modes M and CP and their amplitudes, the growth mode RT0 and its amplitude, the elastic amplitude, E, and their sum, Σ, are shown by solid lines, the branch points of the continuous modes D and RT and their amplitudes by dashed lines. The normalizations are as for Fig. 1. In contrast to Fig. 1(c), the contribution due to the load is included in (d).
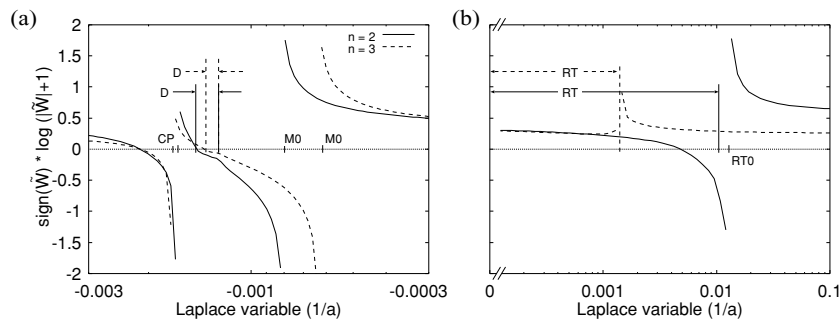

Figure 7. Vertical displacement $\tilde{W}(s)$ of approximation C2 for normalized wavenumber $n = 2$ (solid) and $n = 3$ (dashed) in logarithmic scale for negative and positive s, respectively. The non-analytic regions are marked by arrows and the modes by their symbols.

sphere (Section 5). For the chosen parametrization (Table 1) and for $n < 3$, another root in det **M** appears as a growth mode RT0. For increasing wavenumber, this pole moves towards $s_1^{\mathcal{B}}$. For $n > 3$, it becomes numerically indistinguishable from $s_1^{\mathcal{B}}$ (Fig. 7). Here, we have plotted $\tilde{W}$ as a function of the Laplace variable, s, in order to show the divergent behaviour of the displacement at the poles. For negative values of s, we notice that the amplitudes on the branch cut $\mathcal{C}^{<0}$ remain finite, although the function is non-analytic.

    The amplitude spectrum (Figs 6b–d) for approximation C2 shows several pathological features. In comparison with approximation C1, the vertical amplitude of mode M does not decrease for small wavenumbers and the horizontal amplitude is zero at the surface. Mode CP behaves similarly to that of approximation C1, the continuous mode D has a small positive amplitude. For the local incremental gravity, the sum
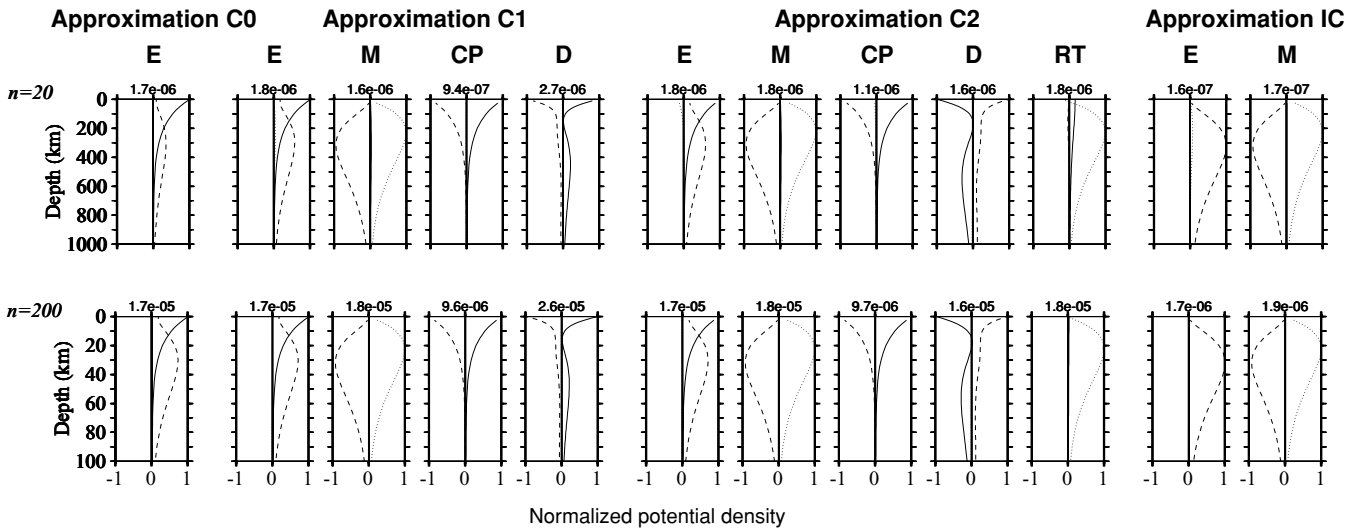
Figure 8. Normalized potential densities for approximations C1, C2 and IC for the elastic amplitude and the amplitudes of the individual relaxation and continuous modes as denoted at the top. For normalized wave numbers $n = 20$ and 200, the contributions of bulk, $\mathcal{E}_\kappa$ (solid), shear, $\mathcal{E}_\mu$ (dashed), and gravity, $\mathcal{E}_\rho$ (dotted), are shown as functions of depth. At the top of each plot, the maximum value is given.

of all amplitudes, Σ, is negative. This means that the mass deficit produced by the vertical displacement is larger than needed for hydrostatic equilibrium. As can be shown from the residue theorem for this approximation, the sum of the elastic amplitude and the amplitudes of the relaxation modes must be equal to that of the growth modes (Hanyk *et al.* 1999). Furthermore, because of $s_4^{\mathcal{B}} = 0$, the function is non-analytic at $s = 0$ and, therefore, the inviscid amplitude does not exist. The destabilizing behaviour at $n \to n_{\text{crit}}$ exists for all discussed field quantities.

We interpret the physical meaning of these modes by discussing the potential densities (e.g. Tromp & Mitrovica 1999b; Klemann & Wolf 1999), which are given by eqs (C8)–(C10). Fig. 8 shows the potential densities for the contributions of E_κ, E_μ and E_ρ as functions of depth for wavenumbers $n = 20$ and 200 and for the elastic and viscous amplitudes. Whereas, for all approximations, mode M is dominated by E_μ and E_ρ and, therefore, represents shear relaxation arising from gravity, mode CP is dominated by E_μ and E_κ, and, thus, represents shear relaxation caused by compression. The continuous mode D behaves similarly to CP, but has a larger depth penetration. For this mode and approximation C2, the signs of E_μ and E_κ are opposite to those for mode CP and for modes D, CP of approximation C1. The continuous growth mode RT shows only small values for compression and shear, but dominant contributions for gravity. Furthermore, the different contributions to mode RT do not cancel if we integrate them with respect to depth, which is in contrast to the behaviour of the relaxation modes. This is as expected for a Rayleigh–Taylor instability driven by an unstable density gradient.

To study the instability in the time domain, we consider a Heaviside excitation of the displacement. Fig. 9 shows the evolution of the horizontal and vertical surface displacements for wavenumbers $n = 2, 20$ and 200, respectively. The vertical displacement relaxes on timescales
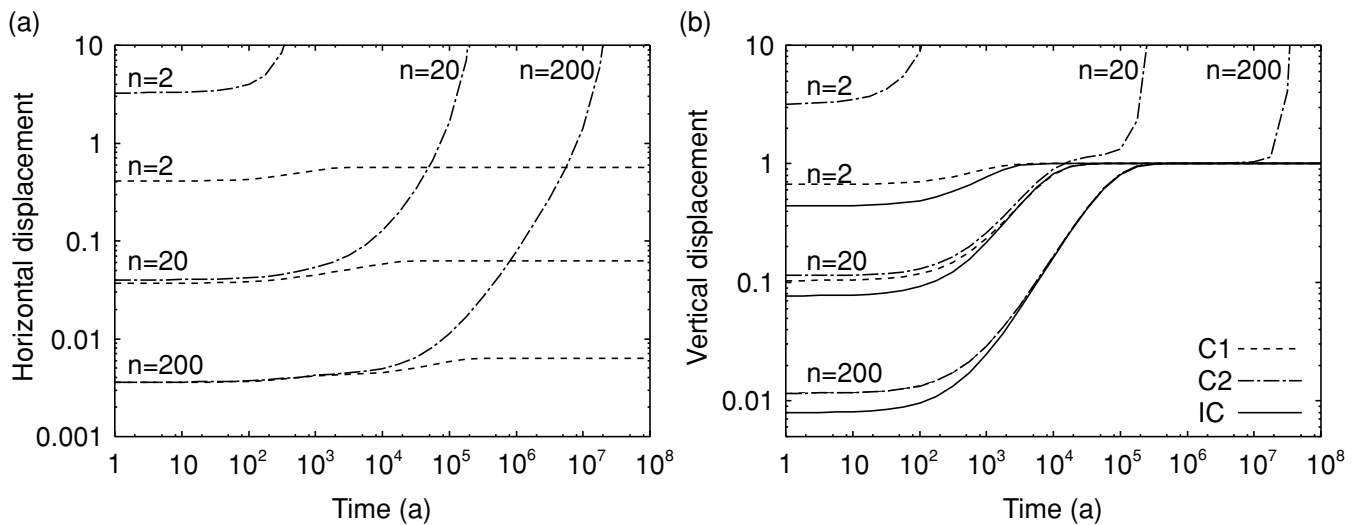

Figure 9. Time evolution of (a) horizontal displacement and (b) vertical displacement after Heaviside loading at $t = 0$ for approximations C1, C2 and IC and for wavenumbers $n = 2, 20$ and 200, respectively.

Table 2. Parameter values for homogeneous plane-Earth model in correspondence with Hanyk *et al.* (1999).

$\rho^{(0)}$ (kg m^{-3})	κ (GPa)	μ^{E} (GPa)	η (Pa s)
5517	449.8	145.2	10^{21}

governed by the dominant mode M. At the inviscid limit, the displacements for approximations C1 and IC are equal to one and correspond to hydrostatic equilibrium. For approximation C2, after relaxation of the contribution due to mode M, the displacement is slightly larger than one. Furthermore, for $n \leq 2$, the elastic displacement becomes singular. For $2 \leq n \leq 20$, stress relaxation continues to support instability. For $n \geq 20$, a period of transient equilibrium develops, the duration of which increases with increasing wavenumber. For small loads and small loading times, the instability is therefore not observed. This explains why Purcell (1998) did not find any instabilities for approximation C2. The differences in the horizontal displacements are more significant (Fig. 9a). As mentioned, the horizontal displacement is zero for approximation IC. Because of the rather small amplitudes of modes CP, D and M for approximation C1, the inviscid amplitude differs only slightly from the elastic amplitude. For approximation C2, the Rayleigh–Taylor instability governs the evolution of instability.

5 RELATION TO SPHERICAL SOLUTIONS

To compare our results with those of Vermeersen *et al.* (1996b) and Hanyk *et al.* (1999) for a homogeneous, viscoelastic self-gravitating sphere where all terms are considered in eq. (1), we use a parametrization of the half-space equal to that used by these authors (Table 2). As shown below, the continuous modes found for approximations C1 and C2 are directly related to the discrete relaxation modes D discussed by Vermeersen *et al.* (1996b) and the growth modes RT found by Hanyk *et al.* (1999) for a homogeneous, viscoelastic self-gravitating sphere. Fig. 10 shows the relative positions of the modes for approximation C2 and the modes for the spherical solution (Hanyk *et al.* 1999). The relaxation modes D appear in a narrow band on the negative s-axis with a fundamental mode D0 corresponding to mode CP. The overtones, Dm, are related to spherical Bessel functions defining the depth dependency, and are given by (Hanyk *et al.* 1999, eq. 2):

$$s_n^{Dm} = -\frac{1}{\tau} \frac{\Gamma_n^m \kappa - 1}{\Gamma_n^m (\kappa + \frac{4}{3}\mu^E) - 1}, \qquad \Gamma_n^m := \frac{[(2m + n - 1)\pi]^2}{\rho^{(0)} g^{(0)} a}. \tag{25}$$

For $m \to \infty$, the overtones converge to $s_\infty^D := -1/\tau[\kappa/(\kappa + \frac{4}{3}\mu^E)]_+$, which is equal to s_3^B for approximations C1 and C2, see eqs (B3) and (B7). For $n \to \infty$, s_n^{Dm} converge $\propto n^2$ to s_∞^D and, similarly, $\mathrm{Re}\{s_{1,2}^B\}$ for approximation C1 and s_2^B for approximation C2 converge $\propto n^2$ to s_3^B, see eqs (B2) and (B5).

The growth modes RT for spherical geometry are also related to spherical Bessel functions with the approximation

$$s_n^{RTm} = \frac{n(n+1)}{\kappa \eta} \left(\frac{1}{\Gamma_n'^m} \right)^2, \qquad \Gamma_n'^m := \frac{[(2m + n)\pi]^2}{4\rho^{(0)} g^{(0)} a}, \tag{26}$$

which holds for n, m sufficiently large (Hanyk *et al.* 1999, eq. 1). Fig. 11 shows the growth time of mode RT1 together with the behaviour of s_1^B for approximation C2. In eq. (26), the upper bound of the modes RTm is the fundamental mode RT1 with $s_n^{RT1} > 0$. Because we have neglected term IV in approximation C2, the fundamental mode RT1 and the upper branch cut s_n^{RTm} should not coincide. The limit of s_n^{RTm} for $m \to \infty$ is 0 and corresponds to $s_4^B = 0$, which represents the case $\epsilon \to \infty$ in eq. (A22). For $n \to \infty$, s_n^{RTm} converges $\propto n^2 \to 0$. This corresponds to the behaviour of s_1^B, which, for $n \to \infty$, converges $\propto n^2 \to 0$ according to eq. (B5). An interesting feature is the influence of shear relaxation on mode RT. Considering eqs (3), (B5) and (B6),

$$s_1^B = \frac{2\kappa}{\eta} \left[\Gamma \left(1 + \sqrt{1 + \frac{16}{3}\Gamma^{-1}} \right) - \frac{2\kappa}{\mu^E} \right]^{-1}, \qquad \Gamma := \left[\frac{\kappa n}{\rho^{(0)} g^{(0)} a} \right]^2 \tag{27}$$

we observe that the influence of μ^E is only significant for small n. Defining s_1^{B*} by neglecting the term $-2\kappa/\mu^E$ in eq. (27), a difference with s_1^B only appears in the vicinity of the stability margin, n_{crit}, given in eq. (21), where the shear relaxation dominates s_1^B. This is shown in
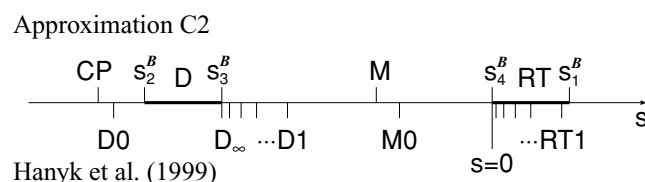
Figure 10. Positions of modes on an unscaled s-axis for the spherical model by Hanyk *et al.* (1999) and of modes for approximation C2.
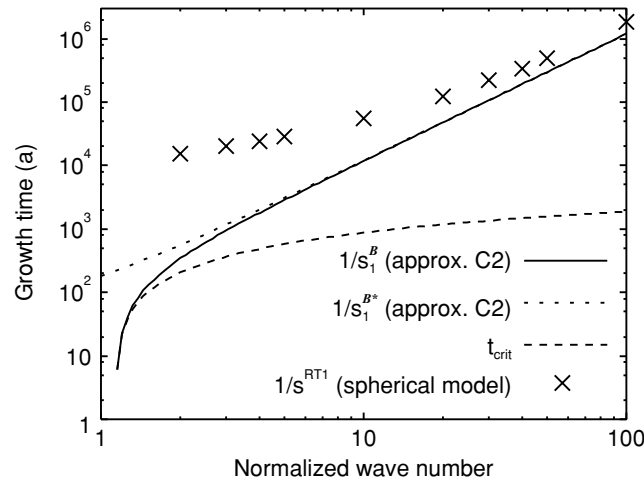
Figure 11. Growth times of mode RT1 for a compressible viscoelastic sphere after Hanyk *et al.* (1999) (crosses) and in the same parametrization (Table 2) for approximation C2. The diagram shows the branch point $1/s_1^B$ (solid line), the branch point $1/s_1^{B*}$, where the influence of μ^E is neglected (short dashes), and the time t_{crit} when the relaxation function $m(t)$ reaches the stability margin μ_{crit} (long dashes).

Fig. 11, where we have plotted $t_{crit} := \tau \ln(\mu^E/\mu_{crit})$. This is the time when the shear-relaxation function $m(t)$ reaches the lower bound μ_{crit} for a stable elastic continuum. According to eq. (21), we have

$$\mu_{crit} = \frac{3}{8}\kappa \left(\sqrt{1 + \frac{16}{3}\Gamma^{-1}} - 1 \right). \tag{28}$$

We therefore conclude that the behaviour of the branch cut $\mathcal{C}^{>0}$ is mainly determined by the viscous flow of the Rayleigh–Taylor instability and, in the vicinity of the stability margin, by additional shear relaxation.

6 DISCUSSION

We have shown that the analogy between the solutions for load-induced perturbations of compressible, viscoelastic, spherical and plane-Earth models with respect to conventional relaxation modes can be extended to non-conventional modes, so that the discrete modes D and RT of spherical Earth models correspond to continuous modes of plane-Earth models. Unlike the approach in Vermeersen *et al.* (1996b), Hanyk *et al.* (1999) and Vermeersen & Mitrovica (2000), where only the roots of the determinant function along the real *s*-axis are studied, our half-space problem involves singularities and branch cuts in the complex *s*-plane. (As was demonstrated for approximation C1, the existence of a branch cut off the real *s*-axis actually gave rise to the relaxation mode D.) Mode D is a consequence of the assumption of homogeneous, compressible regions and describes a readjustment due to elastic compression and viscoelastic shear relaxation. For approximation C1, the vertical displacement associated with mode D is directed upward. However, this is overcompensated by mode CP, for which the displacement is directed downward. In contrast, mode RT only appears if internal buoyancy is included. This mode is the driving mechanism for the instability arising for approximation C2. Mode RT is governed by the gravity potential, $\mathcal{E}_\rho$; the influence of viscoelastic shear relaxation, $\mathcal{E}_\mu$, and of elastic compression, $\mathcal{E}_\kappa$, is negligible. Also, the energy balance shows disequilibrium for approximation C2, whereas, for approximation C1, it is closed. In contrast to Purcell (1998), who did not find instabilities, we have analysed the instability of approximation C2 in detail. For wavenumbers near 100, the instability develops after approximately 10^6a. Therefore, we advise not to use approximation C2. If approximation C1 is used, the horizontal displacement and the local incremental gravity do not vanish at the inviscid limit, as expected from the behaviour of an inviscid fluid. At the elastic limit, both compressible approximations are questionable only for very small wavenumbers. However, for long-wavelength perturbations, the curvature of the Earth must be considered, i.e. plane-Earth models are no longer valid regardless of the chosen approximation. For very large wavenumbers, the absolute differences between the compressible approximations tend to zero, and, thus, the influence of gravity becomes negligible. Compressibility is mandatory when modelling the horizontal displacements and produces an offset with respect to incompressibility in the vertical displacement $\propto \frac{1}{2} - \nu$. For the local incremental gravity, the additional mass deficit due to the offset in the vertical displacement is nearly compensated by the density increase due to compression.

Consequently, a homogeneous reference state should not be used for compressible viscoelastic perturbations, whereas for elastic perturbations, this assumption is valid if limited to excitations of small wavelengths.

REFERENCES

Alterman, Z., Jarosch, H. & Pekeris, C.L., 1959. Oscillations of the Earth, *Proc. R. Soc. Lond., Ser. A,* **252,** 80–95.

Arfken, G., 1985. *Mathematical Methods for Physicists,* 3rd edn, Academic, San Diego.

Backus, G. & Gilbert, F., 1961. The rotational splitting of the free oscillations of the Earth, *Proc. Nat. Am. Soc.,* **47,** 362–371.

Bullen, K.E., 1975. *The Earth's Density,* Chapman and Hall, London.

Cathles, L.M., 1975. *The Viscosity of the Earth's Mantle,* Princeton University Press, Princeton.

Farrell, W.E., 1972. Deformation of the Earth by surface loads, *Rev. Geophys.,* **10,** 761–797.

Gantmacher, F.R., 1986. *Matrizentheorie,* Springer-Verlag, Berlin.

Han, D. & Wahr, J., 1995. The viscoelastic relaxation of a realistically stratified Earth, and a further analysis of postglacial rebound, *Geophys. J. Int.,* **120,** 287–311.

Hanyk, L., Matyska, C. & Yuen, D.A., 1999. Secular gravitational instability of a compressible viscoelastic sphere, *Geophys. Res. Lett.,* **26,** 557–560.

Jeans, J.H., 1903. On the vibrations and stability of a gravitating planet, *Proc. R. Soc. Lond., Ser. A,* **201,** 157–184.

Jeffreys, S.H., 1959. *The Earth, Its Origin, History and Physical Constitution,* Cambridge University Press, Cambridge.

Klemann, V. & Wolf, D., 1999. Implications of a ductile crustal layer for the deformation caused by the Fennoscandian ice sheet, *Geophys. J. Int.,* **139,** 216–226.

Landau, L.D. & Lifschitz, E.M., 1989. *Lehrbuch der theoretischen Physik: Elastizitätstheorie,* 6th edn, Akademie-Verlag, Berlin.

Li, G. & Yuen, D.A., 1987. Viscous relaxation of a compressible spherical shell, *Geophys. Res. Lett.,* **14,** 1227–1230.

Love, A.E.H., 1908. The gravitational stability of the Earth, *Phil. Trans. R. Soc. Lond., Ser. A,* **207,** 171–241.

Love, A.E.H., 1911. *Some Problems of Geodynamics,* Dover, New York.

Martinec, Z., Thoma, M. & Wolf, D., 2001. Material versus local incompressibility and its influence on glacial-isostatic adjustment, *Geophys. J. Int.,* **144,** 136–156.

Maupin, V., 1996. The radiation modes of a vertically varying half-space: a new representation of the complete Green's function in terms of modes, *Geophys. J. Int.,* **126,** 762–780.

Peltier, W.R., 1974. The impulse response of a Maxwell Earth, *Rev. Geophys. Space Phys.,* **12,** 649–669.

Peltier, W.R., 1976. Glacial–isostatic adjustment—II. The inverse problem, *Geophys. J. R. astr. Soc.,* **46,** 669–705.

Peltier, W.R., 1985. The Lageos constraint on deep mantle viscosity: results from a new normal mode method for the inversion of viscoelastic relaxation spectra, *J. geophys. Res.,* **90,** 9411–9421.

Plag, H.-P. & Jüttner, H.-U., 1995. Rayleigh–Taylor instabilities of a self-gravitating Earth, *J. Geodyn.,* **20,** 267–288.

Purcell, A., 1998. The significance of pre-stress advection and internal buoyancy in the flat-Earth formulation, in *Dynamics of the Ice Age Earth: a Modern Perspective,* pp. 105–122, ed. Wu, P., Trans. Tech. Publications, Hetikon.

Rayleigh, L., 1906. On the dilatational stability of the Earth, *Proc. R. Soc. Lond., Ser. A,* **77,** 486–499.

Rümpker, G. & Wolf, D., 1996. Viscoelastic relaxation of a Burgers half-space: implications for the interpretation of the Fennoscandian uplift, *Geophys. J. Int.,* **124,** 541–555.

Sharp, D.H., 1984. An overview of Rayleigh–Taylor instability, *Physica D,* **12,** 3–18.

Singh, S.J., 1970. Static deformation of a multilayered half-space by internal sources, *J. geophys. Res.,* **75,** 3257–3263.

Tromp, J. & Mitrovica, J.X., 1999a. Surface loading of a viscoelastic Earth—I. General theory, *Geophys. J. Int.,* **137,** 847–855.

Tromp, J. & Mitrovica, J.X., 1999b. Surface loading of a viscoelastic Earth—II. Spherical models, *Geophys. J. Int.,* **137,** 856–872.

Vermeersen, L.L.A. & Mitrovica, J.X., 2000. Gravitational stability of spherical self-gravitating relaxation models, *Geophys. J. Int.,* **142,** 351–360.

Vermeersen, L.L.A., Sabadini, R. & Spada, G., 1996a. Analytical viscoelastic relaxation models, *Geophys. Res. Lett.,* **23,** 697–700.

Vermeersen, L.L.A., Sabadini, R. & Spada, G., 1996b. Compressible rotational deformation, *Geophys. J. Int.,* **126,** 735–761.

Wieczerkowski, K., 1999. *Gravito-Viskoelastodynamik für verallgemeinerte Rheologien mit Anwendung auf den Jupitermond Io und die Erde,* Series C, No. 515, Verlag der Bayerischen Akademie der Wissenschaften, München.

Wilcox, C.H., 1984. *Sound Propagation in Stratified Fluids,* Springer-Verlag, New York.

Wolf, D., 1985a. The normal modes of a layered, incompressible Maxwell half-space, *J. Geophys.,* **57,** 106–117.

Wolf, D., 1985b. The normal modes of a uniform, compressible Maxwell half-space, *J. Geophys.,* **56,** 100–105.

Wolf, D., 1991a. Viscoelastodynamics of a stratified compressible planet: incremental field equations and short- and long-time asymptotes, *Geophys. J. Int.,* **104,** 401–417.

Wolf, D., 1991b. Boussinesq's problem of viscoelasticity, *TerraNova,* **3,** 401–407.

Wolf, D., 1997. *Gravitational Viscoelastodynamics for a Hydrostatic Planet,* Series C, No. 452, Verlag der Bayerischen Akademie der Wissenschaften, München.

Wolf, D. & Kaufmann, G., 2000. Effects due to compressional and compositional density stratification on load-induced Maxwell-viscoelastic perturbations, *Geophys. J. Int.,* **140,** 51–62.

Wolf, D. & Li, G., 2002. Compressible viscoelastic Earth models based on Darwin's law, in *Glacial Isostatic Adjustment and the Earth System: Sea-Level, Crustal Deformation, Gravity and Rotation,* pp. 275–292, eds Mitrovica, J.X. & Vermeersen, L.L.A., American Geophysical Union, Washington, DC.

Wu, P., 1978. Response of a Maxwell Earth to applied surface mass loads: glacial isostatic adjustment, *MSc thesis,* University of Toronto.

Wu, P., 1992. Viscoelastic versus viscous deformation and the advection of pre-stress, *Geophys. J. Int.,* **108,** 136–142.

Wu, P. & Ni, Z., 1996. Some analytical solutions for the viscoelastic gravitational relaxation of a two-layer non-self-gravitating incompressible spherical Earth, *Geophys. J. Int.,* **126,** 413–436.

Wu, P. & Peltier, W.R., 1982. Viscous gravitational relaxation, *Geophys. J. R. astr. Soc.,* **70,** 435–485.

Wu, J. & Yuen, D.A., 1991. Post-glacial relaxation of a viscously stratified compressible mantle, *Geophys. J. Int.,* **104,** 331–349.

APPENDIX A: SOLUTION OF THE FUNDAMENTAL SYSTEM

In the following, the solutions of the fundamental system (11) for the approximations considered are given.

Approximation C0:

$$\mathbf{L}(z) = \begin{pmatrix} 1 & 2\dfrac{\delta}{k}+z & -1 & 2\dfrac{\delta-1}{k}-z \\[2mm] 1 & k^{-1}+z & 1 & k^{-1}+z \\[1mm] 2k\tilde{\mu} & 2\tilde{\mu}(1+\delta+kz) & 2k\tilde{\mu} & 2\tilde{\mu}(1-\delta+kz) \\[1mm] 2k\tilde{\mu} & 2\tilde{\mu}(\delta+kz) & -2k\tilde{\mu} & 2\tilde{\mu}(\delta-2-kz) \end{pmatrix} \tag{A1}$$

with

$$\delta := \frac{\tilde{\lambda} + 2\tilde{\mu}}{\tilde{\lambda} + \tilde{\mu}} \tag{A2}$$

and the twofold eigenvalues

$$m_1 = k, \quad m_2 = -k. \tag{A3}$$

Using eq. (13) in eqs (14) and (15) for the displacement and eqs (19) and (20) for the local incremental gravity, we find at the surface

$$\tilde{U} = \frac{1}{2k\tilde{\mu}} \frac{\tilde{\mu}}{\tilde{\lambda} + \tilde{\mu}} g^{(0)} \tilde{\Sigma}, \tag{A4}$$

$$\tilde{W} = \frac{1}{2k\tilde{\mu}} \frac{\tilde{\lambda} + 2\tilde{\mu}}{\tilde{\lambda} + \tilde{\mu}} g^{(0)} \tilde{\Sigma} \tag{A5}$$

$$\tilde{G} = 2\pi\gamma \left(1 - \frac{\rho^{(0)} g^{(0)}}{2k\tilde{\mu}} \right) \tilde{\Sigma} \tag{A6}$$

and, for the elastic limit,

$$U^{\mathrm{E}} = \frac{1 - 2\nu}{2\mu^{\mathrm{E}} k} g^{(0)} \Sigma, \tag{A7}$$

$$W^{\mathrm{E}} = \frac{1 - \nu}{\mu^{\mathrm{E}} k} g^{(0)} \Sigma, \tag{A8}$$

$$G^{\mathrm{E}} = 2\pi\gamma \left(1 - \frac{\rho^{(0)} g^{(0)}}{2k\mu^{\mathrm{E}}} \right) \Sigma. \tag{A9}$$

Approximation C1:

$$\mathbf{L} = \begin{pmatrix} 1 + 2\delta & m_2/k + 2\epsilon & -1 + 2\delta & m_4/k + 2\epsilon \\ 1 & 1 & 1 & 1 \\ 2\tilde{\mu}k(1 + \delta) & 2\tilde{\mu}k & 2\tilde{\mu}k(1 - \delta) & 2\tilde{\mu}k \\ 2\tilde{\mu}k - 2\tilde{\lambda}k\delta & 2\tilde{\mu}m_2 - 2\tilde{\lambda}k\epsilon & -2\tilde{\mu}k - 2\tilde{\lambda}k\delta & 2\tilde{\mu}m_4 - 2\tilde{\lambda}k\epsilon \end{pmatrix} \tag{A10}$$

with

$$\delta = \frac{\rho^{(0)} g^{(0)}}{2k(\tilde{\lambda} + \tilde{\mu})}, \qquad \epsilon = \frac{\rho^{(0)} g^{(0)}}{2k(\tilde{\lambda} + 2\tilde{\mu})} \tag{A11}$$

and the simple eigenvalues

$$m_1 = k, \qquad m_2 = k(\sqrt{1 + \epsilon^2} - \epsilon), \qquad m_3 = -k, \qquad m_4 = -k(\sqrt{1 + \epsilon^2} + \epsilon). \tag{A12}$$

at the surface, the displacement and local incremental gravity are

$$\det \mathbf{M} = (2\tilde{\mu}k)^2 \left[1 + \epsilon \left(\frac{\rho^{(0)} g^{(0)}}{2k\tilde{\mu}} - \frac{\tilde{\mu}}{\tilde{\lambda} + \tilde{\mu}} \right) - \sqrt{1 + \epsilon^2} (1 - \delta) \right], \tag{A13}$$

$$\tilde{U} = \frac{2\tilde{\mu}k}{\det \mathbf{M}} \left[\delta - \left(1 + \epsilon - \sqrt{1 + \epsilon^2} \right) (1 - \delta) \right] g^{(0)} \tilde{\Sigma}, \tag{A14}$$

$$\tilde{W} = \frac{2\tilde{\mu}k}{\det \mathbf{M}} \delta g^{(0)} \tilde{\Sigma}, \tag{A15}$$

$$\tilde{G} = 2\pi\gamma \left[1 - \frac{2\tilde{\mu}k}{\det \mathbf{M}} \frac{2\rho^{(0)} g^{(0)} \epsilon (1 - \delta)}{1 + \epsilon + \sqrt{1 + \epsilon^2}} \right] \tilde{\Sigma} \tag{A16}$$

and, for the elastic limit with $\epsilon \ll 1$ and $\delta \ll 1$,

$$U^{\mathrm{E}} \simeq \frac{1 - 2\nu}{2\mu^{\mathrm{E}} k + \rho^{(0)} g^{(0)}} g^{(0)} \Sigma, \tag{A17}$$

$$W^{\mathrm{E}} \simeq \frac{2(1 - \nu)}{2\mu^{\mathrm{E}} k + \rho^{(0)} g^{(0)}} g^{(0)} \Sigma, \tag{A18}$$

$$G^{\mathrm{E}} \simeq 2\pi\gamma \left[1 - \frac{(1 - \delta)\rho^{(0)} g^{(0)}}{2\mu^{\mathrm{E}} k + \rho^{(0)} g^{(0)}} \right] \Sigma. \tag{A19}$$

Approximation C2:

$$
\mathbf{L} = \begin{pmatrix}
\gamma + \epsilon & \gamma\dfrac{m_1}{k} - \delta & k\tilde{\mu}\left[(2\gamma + \epsilon)\dfrac{m_1}{k} - \delta\right] & k\tilde{\mu}(2\gamma + \epsilon) - \rho^{(0)}g^{(0)}\dfrac{m_1}{k} \\[2mm]
\gamma - \epsilon & \gamma\dfrac{m_2}{k} - \delta & k\tilde{\mu}\left[(2\gamma - \epsilon)\dfrac{m_2}{k} - \delta\right] & k\tilde{\mu}(2\gamma - \epsilon) - \rho^{(0)}g^{(0)}\dfrac{m_2}{k} \\[2mm]
\gamma + \epsilon & -\gamma\dfrac{m_1}{k} - \delta & k\tilde{\mu}\left[-(2\gamma + \epsilon)\dfrac{m_1}{k} - \delta\right] & k\tilde{\mu}(2\gamma + \epsilon) + \rho^{(0)}g^{(0)}\dfrac{m_1}{k} \\[2mm]
\gamma - \epsilon & -\gamma\dfrac{m_2}{k} - \delta & k\tilde{\mu}\left[-(2\gamma - \epsilon)\dfrac{m_2}{k} - \delta\right] & k\tilde{\mu}(2\gamma - \epsilon) + \rho^{(0)}g^{(0)}\dfrac{m_2}{k}
\end{pmatrix}^{\mathrm{T}}
\tag{A20}
$$

in its transposed form with

$$
\gamma := \frac{\tilde{\lambda} + \tilde{\mu}}{\tilde{\lambda} + 2\tilde{\mu}}, \qquad \delta := \frac{\rho^{(0)}g^{(0)}}{k(\tilde{\lambda} + 2\tilde{\mu})}, \qquad \epsilon := \frac{\rho^{(0)}g^{(0)}}{k\sqrt{\tilde{\mu}(\tilde{\lambda} + 2\tilde{\mu})}}
\tag{A21}
$$

and the simple eigenvalues

$$
m_1 = k\sqrt{1 + \epsilon}, \quad m_2 = k\sqrt{1 - \epsilon}, \quad m_3 = -k\sqrt{1 + \epsilon}, \quad m_4 = -k\sqrt{1 - \epsilon}.
\tag{A22}
$$

At the surface, the displacement is given by

$$
\det\mathbf{M} = -2(k\tilde{\mu})^2\left[(2\gamma^2 - \epsilon^2)(\sqrt{1 + \epsilon} - \sqrt{1 - \epsilon}) - \epsilon\left(\delta - \frac{\rho^{(0)}g^{(0)}}{k\tilde{\mu}}\sqrt{1 - \epsilon^2}\right)\right],
\tag{A23}
$$

$$
\tilde{U} = \frac{k\tilde{\mu}g^{(0)}\tilde{\Sigma}}{\det\mathbf{M}}\left[(2\gamma^2 - \epsilon^2)(\sqrt{1 + \epsilon} - \sqrt{1 - \epsilon}) - \gamma\epsilon(\sqrt{1 + \epsilon} + \sqrt{1 - \epsilon}) - 2\epsilon\delta\right],
\tag{A24}
$$

$$
\tilde{W} = \frac{-k\tilde{\mu}g^{(0)}\tilde{\Sigma}}{\det\mathbf{M}}\left[\gamma\delta(\sqrt{1 + \epsilon} - \sqrt{1 - \epsilon}) + \epsilon\delta(\sqrt{1 + \epsilon} + \sqrt{1 - \epsilon}) + 2\gamma\epsilon\sqrt{1 - \epsilon^2}\right].
\tag{A25}
$$

We do not show the expression for the local incremental gravity because of its length. For the elastic limit and $\epsilon \ll 1$ and $\delta \ll 1$, we obtain

$$
U^{\mathrm{E}} \simeq \frac{1 - 2\nu + 4(1 - \nu)^2\delta}{2\mu^{\mathrm{E}}k + 2(1 - \nu)\rho^{(0)}g^{(0)}}g^{(0)}\Sigma,
\tag{A26}
$$

$$
W^{\mathrm{E}} \simeq \frac{2(1 - \nu) + (5 - \nu)\gamma^{-1}\delta}{2\mu^{\mathrm{E}}k + 2(1 - \nu)\rho^{(0)}g^{(0)}}g^{(0)}\Sigma,
\tag{A27}
$$

$$
G^{\mathrm{E}} \simeq 2\pi\gamma\left[1 - \frac{\rho^{(0)}g^{(0)}}{2\mu^{\mathrm{E}}k + 2(1 - \nu)\rho^{(0)}g^{(0)}}\right]\Sigma.
\tag{A28}
$$

Approximation IC:

$$
\mathbf{L}(z) = \begin{pmatrix}
1 & z & -1 & -z \\[2mm]
1 & -\dfrac{1}{k} + z & 1 & \dfrac{1}{k} + z \\[2mm]
2k\tilde{\mu} & 2k\tilde{\mu}z & 2k\tilde{\mu} & 2k\tilde{\mu}z \\[2mm]
2k\tilde{\mu}(1 - \epsilon) & -2k\tilde{\mu}(1 - \epsilon)\left(\dfrac{1}{k} - z\right) & -2k\tilde{\mu}(1 + \epsilon) & -2k\tilde{\mu}(1 + \epsilon)\left(\dfrac{1}{k} + z\right)
\end{pmatrix}
\tag{A29}
$$

with

$$
\epsilon := \frac{\rho^{(0)}g^{(0)}}{2k\tilde{\mu}}
\tag{A30}
$$

and the twofold eigenvalues

$$
m_1 = k, \qquad m_2 = -k.
\tag{A31}
$$

At the surface, the displacement and local incremental gravity are

$$
\tilde{U} = 0,
\tag{A32}
$$

$$
\tilde{W} = \frac{1}{2k\tilde{\mu} + \rho^{(0)}g^{(0)}}g^{(0)}\tilde{\Sigma},
\tag{A33}
$$

$$
\tilde{G} = 2\pi\gamma\frac{2k\tilde{\mu}}{2k\tilde{\mu} + \rho^{(0)}g^{(0)}}\tilde{\Sigma}
\tag{A34}
$$

and, for the elastic limit,

$$
U^{\mathrm{E}} = 0,
\tag{A35}
$$

$$W^{\mathrm{E}} = \frac{1}{2k\mu^{\mathrm{E}} + \rho^{(0)}g^{(0)}} g^{(0)}\Sigma, \tag{A36}$$

$$G^{\mathrm{E}} = 2\pi\gamma \left(1 - \frac{\rho^{(0)}g^{(0)}}{2k\mu^{\mathrm{E}} + \rho^{(0)}g^{(0)}}\right) \Sigma. \tag{A37}$$

APPENDIX B: NON-ANALYTICITY OF APPROXIMATIONS C1 AND C2

As non-analytic function, $\sqrt{z}$ appears in the solutions for approximations C1 and C2. $\sqrt{z}$ has branch points at $z = 0$ and $z = \infty$ and a branch cut, which is usually defined as the line $z < 0$ where $\sqrt{z}$ is purely imaginary and non-analytic with a phase change of π. To understand its influence on the solutions we mainly focus on the eigenvalues, which appear linearly also in the fundamental systems, $\mathbf{L}$. For the eigenvalues of approximation C1 given in eq. (A12), we note that $z = 1 + \epsilon^2$ is now a complex function of the Laplace variable, s. Rewriting $\sqrt{1 + \epsilon^2} = \sqrt{1 + \epsilon i}\sqrt{1 - \epsilon i}$ the branch points are $\epsilon = \pm i$ and the branch cuts extend from the branch points to infinity along $\epsilon = \pm\alpha\, i$ where $1 < \alpha < \infty$. Inserting (9) into (11) and solving for s we can summarize the analytic behaviour of $\sqrt{1 + \epsilon^2}$ by

$$s(\alpha) = -\frac{1}{\tau}\left(1 + \frac{4}{3}\frac{\mu^{\mathrm{E}}}{\kappa \mp \frac{\rho^{(0)}g^{(0)}}{2k\alpha i}}\right)^{-1} = \begin{cases} s_{1,2}^{\mathcal{B}} & \text{for} \quad \alpha = 1 \\ \mathcal{C}_{1,2} & \text{for} \quad \alpha > 1 \\ s_3^{\mathcal{B}} & \text{for} \quad \alpha = \infty \\ \text{analytic} & \text{for} \quad \alpha < 1 \quad \text{or} \quad \mathrm{Im}\{\alpha\} \neq 0. \end{cases} \tag{B1}$$

In particular, we find

$$\mathrm{Re}\left\{s_{1,2}^{\mathcal{B}}\right\} = -\frac{1}{\tau}\frac{\Gamma\kappa + 1}{\Gamma\left(\kappa + \frac{4}{3}\mu^{\mathrm{E}}\right) + 1}, \quad \Gamma := \left[\frac{2k}{\rho^{(0)}g^{(0)}}\right]^2 \left(\kappa + \frac{4}{3}\mu^{\mathrm{E}}\right) \tag{B2}$$

and

$$s_3^{\mathcal{B}} = -\frac{1}{\tau}\left(\frac{\kappa}{\kappa + \frac{4}{3}\mu^{\mathrm{E}}}\right). \tag{B3}$$

The branch cuts are located on a circular arc with radius $2\mu^{\mathrm{E}}/(3\tau)/(\kappa + 4/3\mu^{\mathrm{E}})$ and centre $-[1 + \kappa/(\kappa + 4/3\mu^{\mathrm{E}})]/(2\tau)$ which is independent of wavenumber, k (Fig. 3). The circle cuts the real axis at the points $s_3^{\mathcal{B}}$ and $-1/\tau$. The point $-1/\tau$ is only reached for $\lim_{k\to 0} s_{1,2}^{\mathcal{B}}$. Because the non-analyticity coincides with $m_{2,4} \in \mathcal{I}$, where $\mathcal{I}$ denotes the set of imaginary numbers, a real linear combination of the eigenvectors given in (13) is a harmonic function of depth and, thus, the non-analytic behaviour coincides with a violation of the regularity condition requiring that all perturbations vanish for $z \to \infty$.

For the eigenvalues of approximation C2, we must distinguish the cases where ϵ is non-analytic according to the square-root $\sqrt{\tilde{\mu}(\tilde{\lambda} + 2\tilde{\mu})}$ in eq. (A21) and where the eigenvalues are non-analytic according to the square-root $\sqrt{1 \pm \epsilon}$ in eq. (A22). In the first case, the square-root has a branch cut for $\tilde{\mu}(\tilde{\lambda} + 2\tilde{\mu}) < 0$. Hence $\epsilon \in \mathcal{I}$ and, therefore, the pairs $m_{1,2}$ and $m_{3,4}$ are complex conjugate. From these, only the pair $m_{3,4}$ with negative real parts is of interest. Because $\mathbf{A}$ is real, $\mathbf{L}_{3,4}$ are also complex conjugate. Considering this behaviour in eqs (13) and (14) for $\Sigma \in \mathcal{R}$, we obtain the solution vector

$$\tilde{\mathbf{Y}} = -g^{(0)}\tilde{\Sigma}\frac{\mathrm{Re}(L_{33}\mathbf{L}_3 e^{m_3 z})}{\mathrm{Re}(L_{33}L_{43})}, \tag{B4}$$

which is a real analytic function that satisfies the regularity condition for $z \to \infty$.

In the second case, $\sqrt{1 - \epsilon}$ is non-analytic for $\epsilon > 1$. This results in $m_{2,4} \in \mathcal{I}$, so that, as for approximation C1, the solution violates the regularity condition. (We need not consider $\sqrt{1 + \epsilon}$, because, according to eq. (A21), ϵ is a square-root function, that is the real part of ϵ must be ≥ 0.) Inserting eq. (9) into eq. (A21) and solving $\epsilon(s) = \alpha > 1$ for s, we summarize the behaviour of the solutions:

$$s(\alpha) = \frac{1}{\tau}\left[\frac{\mu^{\mathrm{E}}}{2\kappa}\Gamma\left(1 \pm \sqrt{1 + \frac{16}{3}\Gamma^{-1}}\right) - 1\right]^{-1} = \begin{cases} s_{1,2}^{\mathcal{B}} & \text{for} \quad \alpha = 1 \\ \mathcal{C}^{>0}, \mathcal{C}^{<0} & \text{for} \quad \alpha > 1 \\ s_{4,3}^{\mathcal{B}} & \text{for} \quad \alpha \to \infty \\ \text{analytic} & \text{for} \quad \alpha < 1 \quad \text{or} \quad \mathrm{Im}\{\alpha\} \neq 0, \end{cases} \tag{B5}$$

where

$$\Gamma = \left[\frac{\kappa k\alpha}{\rho^{(0)}g^{(0)}}\right]^2. \tag{B6}$$

The first subscript denotes the solution for the plus sign and the second for the minus sign. In particular, we find

$$s_3^{\mathcal{B}} = -\frac{1}{\tau}\frac{\kappa}{\kappa + \frac{4}{3}\mu^{\mathrm{E}}}, \qquad s_4^{\mathcal{B}} = 0. \tag{B7}$$

With $s(\alpha)$ monotonic and $s(\alpha) \in \mathcal{R}$ on $\alpha \in (1, \infty)$, the cut lines are (see Fig. 5a)

$$\mathcal{C}^{<0} := \left\{s \in \mathcal{R} \mid s_2^{\mathcal{B}} \leq s \leq s_3^{\mathcal{B}}\right\},$$

$$\mathcal{C}^{>0} := \left\{s \in \mathcal{R} \mid s_4^{\mathcal{B}} \leq s \leq s_1^{\mathcal{B}}\right\}. \tag{B8}$$

The regions of non-analyticity of the solution are excluded numerically by an appropriate integration path.

APPENDIX C: ENERGY POTENTIALS

The energy contributions to the deformation can be calculated directly from (10) using the usual energy functional $\int_V \frac{1}{2}(L\mathbf{u}, \mathbf{u}^*)\,dv^{(0)}$ (e.g. Backus & Gilbert 1961), where L is the differential operator associated with eq. (10). Separating the individual contributions due to excitation, bulk, shear and gravity, we obtain in index notation, where summation over equal indices is implied,

$$\mathcal{E}_\sigma := -\frac{1}{2}\int_{\partial^I\mathcal{X}_+} g^{(0)}\tilde{\sigma}\,\delta_{i3}\tilde{u}_i\,da^{(0)}, \tag{C1}$$

$$\mathcal{E}_\kappa := \int_{\mathcal{X}_+} \frac{\kappa}{2}(\tilde{\epsilon}_{kk})^2\,dv^{(0)}, \tag{C2}$$

$$\mathcal{E}_\mu := \int_{\mathcal{X}_+} \tilde{\mu}\tilde{\epsilon}_{dij}\epsilon_{dij}\,dv^{(0)}, \tag{C3}$$

$$\mathcal{E}_\rho := \begin{cases} -\int_{\mathcal{X}_+} \dfrac{\rho^{(0)}g^{(0)}}{2}\delta_{j3}\tilde{u}_{j,i}\tilde{u}_i\,dv^{(0)} & \text{for approximations C1 and IC} \\[3mm] -\int_{\mathcal{X}_+} \dfrac{\rho^{(0)}g^{(0)}}{2}(\delta_{j3}\tilde{u}_{j,i}\tilde{u}_i - \delta_{j3}\tilde{u}_j\tilde{u}_{i,i})\,dv^{(0)} & \text{for approximation C2,} \end{cases} \tag{C4}$$

where, for $\mathcal{E}_\sigma$, the integral extends over the outer surface, $\partial^I\mathcal{X}_+$, and, for the other contributions, over the viscoelastic half-space, $\mathcal{X}_+$. Considering a spectral load and appropriate normalization, we express the potentials as integrals over depth-dependent potential densities:

$$\mathcal{E}_\kappa = \int_0^\infty E_\kappa(z)\,dz, \tag{C5}$$

$$\mathcal{E}_\mu = \int_0^\infty E_\mu(z)\,dz, \tag{C6}$$

$$\mathcal{E}_\rho = \int_0^\infty E_\rho(z)\,dz \tag{C7}$$

with

$$E_\kappa(z) = \frac{\kappa}{2}(\dot{\tilde{W}} - 2k\tilde{U})^2, \tag{C8}$$

$$E_\mu(z) = \tilde{\mu}\left[(k\tilde{U})^2 + \dot{\tilde{W}}^2 + (\dot{\tilde{U}} + k\tilde{W})^2 - \frac{1}{3}(\dot{\tilde{W}} - 2k\tilde{U})^2\right], \tag{C9}$$

$$E_\rho(z) = -\frac{\rho^{(0)}g^{(0)}}{2}\begin{cases} k\tilde{U}\tilde{W} + \dot{\tilde{W}}\tilde{W} & \text{for approximations C1 and IC} \\ 2k\tilde{U}\tilde{W} & \text{for approximation C2} \end{cases} \tag{C10}$$

and dots for $\partial/\partial z$ (for details see Klemann & Wolf 1999; Tromp & Mitrovica 1999b). The potential of the load,

$$\mathcal{E}_\sigma = -\frac{1}{2}g^{(0)}\tilde{\Sigma}\tilde{W}(z_1), \tag{C11}$$

represents the energy input due to surface loading. For an elastic half-space, eqs (C8)–(C10) represent the energy densities, whereas, for a viscoelastic half-space, they represent potential densities associated with the amplitudes of the individual relaxation and growth modes.